Equivalent channel network model for permeability and electrical conductivity of fracture networks

Clinton D. Van Siclen

Idaho National Engineering and Environmental Laboratory, Idaho Falls, Idaho, USA

Received 31 October 2000; revised 28 October 2001; accepted 2 November 2001; published 4 June 2002.

[1] It is remarkable that the permeability k and electrical conductivity σ of saturated, fractured rock exhibit a power law relationship with exponent r as pressure is applied to the rock. To understand this behavior, the fracture network is viewed as a collection of connected, planar fractures. This allows the construction of algebraic expressions for the transport properties of the fracture network, in which the local effective properties, namely, the hydraulic aperture d_h and the electric aperture d_e of the representative planar fracture (the "equivalent channel"), are distinguished from the network properties (e.g., fracture connectivity) parameterized by the tortuosity factors τ_h and τ_e. This "equivalent channel network model" reproduces the observed power law behavior on the conditions that $d_h^3 \propto d_e^r$ and $\tau_h \propto \tau_e^r$ over the range of applied pressures. The first condition is met, as demonstrated by calculations for a variety of simulated planar fractures using the Reynolds equations for fluid and current flow. The value of the exponent r is found to indicate the degree to which the fracture resembles a porous medium but cannot otherwise identify fracture surface or aperture characteristics. No direct evidence currently exists to support the second condition; however, such a power law relationship has been demonstrated elsewhere for simulated porous media. *INDEX TERMS:* 5104 Physical Properties of Rocks: Fracture and flow; 5139 Physical Properties of Rocks: Transport properties; 5109 Physical Properties of Rocks: Magnetic and electrical properties; 1829 Hydrology: Groundwater hydrology; *KEYWORDS:* fracture(s), network(s), conductivity, permeability, flow, equivalent channel

1. Introduction

[2] The transport properties of fractured rock are determined by the connected void space, that is, by the locally planar fracture segments that comprise the fracture network and by the structure of that network. Fluid and electrical current flow in response to applied fluid pressure and electrical potential gradients, respectively, are thus effectively confined to channels through the rock. The distribution of flux among the channels in the two cases will be different of course, as the electrical current distribution is that which minimizes the total power dissipation (the irreversible conversion of electrical energy into heat) [*Van Baak*, 1999], while there is no corresponding global minimization principle for fluid flow.

[3] Thus it is remarkable that the permeability k and the electrical conductivity σ of fractured rock exhibit a simple power law relationship with exponent r as mechanical pressure is applied to the rock. Single-sample measurements made by various researchers and collected by *Walsh and Brace* [1984] give exponent values over the range $1.5 \leq r \leq 2.8$ for confining pressures causing elastic deformation. In similar measurements on granite samples, *Bernabe* [1988] obtained r values very close to 2. This same power law relationship with exponent very close to 2 is evident in plots made by *Katsube and Walsh* [1987] of the permeability and electrical conductivity of a number of granite samples collected from the same geological site. Clearly, these results contain information about the fracture network. However, because both the permeability and the electrical conductivity are unknown functionals of the fracture morphology and network topology, these experimental results can only be interpreted with the aid of a model.

0148-0227/02/2000JB000057$09.00

[4] An "equivalent channel" model was provided by *Walsh and Brace* [1984] for this purpose. In essence, the fractured rock is represented by a single, smooth channel whose aperture a is effectively reduced for fluid flow. This produces the relations $k = (m^2/b)\,(\phi/\tau^2)$ and $\sigma = \sigma_0\,\phi/\tau^2$, where m is the hydraulic radius, b is a shape factor that equals 3 for cracks, ϕ is the porosity of the sample, τ is the tortuosity of the equivalent channel, and σ_0 is the electrical conductivity of the fluid. With the assumptions that (1) $k(p)$ and $\sigma(p)$ are related by a power law with unknown exponent r (the dependence of k and σ on the applied mechanical pressure p is made explicit here) and (2) a change in the aperture $a(p)$ gives rise to a proportional change in the hydraulic radius $m(p)$, the model yields the relation

$$\frac{\tau(p)^2}{\tau_0^2} = \left[\frac{a(p)}{a_0}\right]^{-(3-r)/(r-1)}, \qquad (1)$$

where the subscript zero refers to some reference pressure. The exponent r is therefore restricted to the range $1 \leq r \leq 3$, just as is seen experimentally; this nice coincidence accounts for the widespread use of this model. Evidently, the observed value of r reflects a sample-specific relationship between the fracture apertures and the network tortuosity as pressure is applied. (*Walsh and Brace* [1984, pp. 9428–9429] conclude that "r is a measure of the sensitivity of the tortuosity to changes in crack aperture: as r approaches 3, tortuosity is nearly independent of aperture, whereas small changes in aperture result in very large changes in tortuosity for samples where r is near unity.")

[5] More recently, research has shown that the fluid and electrical current flow paths through fractured and porous heterogeneous media are not identical [e.g., *Brown*, 1989; *Thompson and Brown*, 1991; *David*, 1993; *Zhang and Knackstedt*, 1995]; that is, the hydraulic tortuosity τ_h is not in general equal to the electric tortuosity τ_e. Because *Walsh and Brace* [1984] rely on a common τ

to connect their expressions for k and σ, their model is fundamentally flawed and its consequences may not be correct. In addition, it is a simple matter to reproduce the experimental results for a single, planar fracture by assuming $k \sim \langle d^3 \rangle$ and $\sigma \sim \langle d \rangle$, where the $\langle d^n \rangle$ are moments of the fracture aperture distribution. Calculations for a wide variety of fractures produce the power law relation $\langle d^3 \rangle \sim \langle d \rangle^s$, with the value of the exponent s decreasing from 3 toward 1 as the fracture percolation threshold is approached. For these and other reasons (e.g., the questionable validity of assumption 2 above), it is desirable to construct an improved equivalent channel model for fractured rock, the goal being to understand the origin of the observed power law relationship between $k(p)$ and $\sigma(p)$.

[6] Section 2 presents the "equivalent channel network" model, which represents the fracture network as a collection of connected, locally planar fractures. The network connectivity is parameterized by the tortuosity factors τ_h and τ_e, while the locally planar (but not "parallel-plate") fractures are characterized by effective hydraulic and electric apertures d_h and d_e, respectively. This is an equivalent channel approach in that these single-valued quantities are taken to be representative of the fracture network as a whole.

[7] Separate models for permeability and electrical conductivity are produced, reflecting the lack of any fundamental relationship between $k(p)$ and $\sigma(p)$. However, the observed power law relationship is reproduced when $d_h^3 \propto d_e^r$ and $\tau_h \propto \tau_e^r$. To assess the validity of the first condition (relating the effective apertures), section 3 presents stochastic calculations of the transport properties of single, planar fractures characterized by average aperture, fracture surface roughness, and fracture surface height variance. Section 4 addresses the second condition (relating the network tortuosity factors) and provides some last comments.

2. Derivation of the Equivalent Channel Network Model

[8] The electrical conductance g_1 of a single, fluid-filled, planar fracture of width w and length L is given by

$$g_1 = \sigma_0 \frac{d_e w}{L}, \tag{2}$$

where d_e is the aperture of a parallel-plate fracture that produces the same current as the planar fracture for a given potential difference applied across the length of the fracture (this is, in fact, the definition of the electric aperture), and σ_0 is the conductivity of the fluid. Then the electrical conductivity σ_1 of the single, planar fracture is

$$\sigma_1 = \frac{g_1 L}{\langle d \rangle w} = \sigma_0 \frac{d_e}{\langle d \rangle}, \tag{3}$$

where $\langle d \rangle$ is the average aperture of the planar fracture. As expected, $\sigma_1 = \sigma_0$ for a fracture with smooth, parallel surfaces ($d_e = \langle d \rangle$).

[9] Now consider a network of such fractures in a configuration where all are oriented parallel to an applied potential gradient. The electrical conductivity of this system is $\phi_0\ \sigma_1$, where ϕ_0 is the volume fraction of this set of planar fractures. (Note that a fracture network necessarily includes the medium in which the fractures are embedded; this is in contrast to the "disembodied" single fracture having electrical conductivity σ_1 and permeability k_1.)

[10] A more realistic fracture network is created by relaxing this restriction on the fracture orientation and, additionally, allowing the fractures to bend while remaining locally planar. The conductivity σ of the network is then reduced to

$$\sigma = \frac{\phi_0 \sigma_1}{\tau} = \frac{\sigma_0 \phi_0}{\tau} \frac{d_e}{\langle d \rangle}, \tag{4}$$

where the factor τ accounts for the increased current path lengths. This expression for σ should be compared with that derived by *Walsh and Brace* [1984].

[11] It is now convenient to use the relation $N_A = \phi_0 / (\langle d \rangle\ w)$, where N_A is the areal number density of fractures intersecting a cross section of the material perpendicular to the applied potential gradient (this assumes all fractures run the length of the sample; N_A is reduced when this is not the case). Of importance to this derivation is the fact that N_A is independent of the fracture geometry and network topology and hence independent of applied pressure. The electrical conductivity of the fracture network is then

$$\sigma = N_A \sigma_0 \frac{d_e w}{\tau_e}. \tag{5}$$

In equation (5) the electric aperture d_e is characteristic of the locally planar fracture segments comprising the network, and τ_e may be regarded as a current path tortuosity factor determined by the network structure (since $\tau_e = 1$ for a network composed of planar fractures oriented parallel to an applied electric field and increases for increasingly complex fracture networks).

[12] An analogous expression may be derived for the permeability k of the fracture network. In this case, the hydraulic conductance h_1 of a single, planar fracture is given by

$$h_1 = \frac{d_h^3 w}{12 L}, \tag{6}$$

where d_h is the aperture of a parallel-plate fracture that produces the same volume flow rate as the planar fracture for a given fluid pressure difference applied across the length of the fracture. Then the hydraulic conductivity k_1 of the fracture is

$$k_1 = \frac{h_1 L}{\langle d \rangle w} = \frac{d_h^3}{12 \langle d \rangle}. \tag{7}$$

The analogue of equation (4) is the relation

$$k = \frac{\phi_0}{\tau} \frac{d_h^3}{12 \langle d \rangle}, \tag{8}$$

which should be compared with the expression for k derived by *Walsh and Brace* [1984], while the analogue of equation (5) is the relation

$$k = N_A \frac{d_h^3 w}{12 \tau_n}. \tag{9}$$

In equation (9) the hydraulic aperture d_h is characteristic of the locally planar fracture segments comprising the network, and τ_h may be regarded as a fluid flow path tortuosity factor determined by the network structure. The factors τ_h and τ_e will not, in general, be equal, since the distributions of fluid and electric flux among the flow paths through a complex fracture network are different.

[13] Equations (5) and (9) for σ and k, respectively, can be combined to give the identity

$$k \propto \sigma^r \frac{d_h^3}{d_e^r} \frac{\tau_e^r}{\tau_h}, \tag{10}$$

where the proportionality constant containing σ_0, N_A, and w is unaffected by pressure. Then $k(p) \propto \sigma(p)^r$ when both ratios d_h^3/d_e^r and τ_e^r/τ_h are slowly varying over the range of applied pressures. Section 3 shows that the first condition is indeed met for single, planar fractures and relates the value of the exponent r to the

fracture geometry. (Both conditions are obviously met with $r = 3$ for the special case of a network consisting of a single, parallel-plate fracture.)

3. Calculation of the Transport Properties of Planar Fractures

[14] The fluid permeability and electrical conductivity of single, computer-generated fractures may be straightforwardly obtained by solving the Navier-Stokes equations [*Mourzenko et al.*, 1995; *Zhang et al.*, 1996] and the Laplace equation [*Volik et al.*, 1997; *Mourzenko et al.*, 1999], respectively, over the three-dimensional interior space of the fracture. However, these calculations are computationally intensive, which severely limits the number of fractures that can be considered and the length scale over which surface roughness can be created.

[15] The approach taken here is inspired by the parallel-plate model for a fracture. For this model, where the fracture surfaces are smooth and parallel, the steady state solution of the Navier-Stokes equations for laminar flow yields the "cubic law"; that is, the volume flow rate $\mathbf{q}$ is proportional to the cube of the aperture d. For planar fractures with rough surfaces, this cubic law is assumed to hold locally:

$$\mathbf{q}(\mathbf{r}) = -\delta \frac{d(\mathbf{r})^3}{12\mu} \nabla p(\mathbf{r}), \tag{11}$$

where the two-dimensional vector $\mathbf{r}$ lies in the plane of the fracture, $\mathbf{q}(\mathbf{r})$ is the volume of fluid discharged per unit time through the cross-sectional area $\delta\, d(\mathbf{r})$, μ is the fluid viscosity, and p is the fluid pressure. The condition of fluid incompressibility, $\nabla \bullet \mathbf{q}(\mathbf{r}) = 0$, then leads to the Reynolds equation for fluid flow,

$$\nabla \bullet \left(d^3 \nabla p\right) = 0. \tag{12}$$

Two observations may be made. First, equation (12) is simply a steady state diffusion equation with a spatially dependent diffusion coefficient, and so can be solved by a variety of conventional methods. Second, equation (11) may be regarded as a microscopic counterpart to Darcy's law,

$$\mathbf{Q} = -\frac{K}{\mu} \nabla P, \tag{13}$$

which expresses the linear relationship between the macroscopic volumetric flow rate $\mathbf{Q}$ through a porous system and the applied fluid pressure gradient ∇P. The proportionality constant K, which is here the effective permeability k_1 of the planar fracture, is to be determined.

[16] This Reynolds equation approach to obtaining flow properties of rough fractures has been used by *Patir and Cheng* [1978], *Brown* [1987], *Moreno et al.* [1988], *Brown* [1989], *Thompson and Brown* [1991], and *Zimmerman et al.* [1991], who solved equation (12) for the local fluid pressures by a finite difference method. More recent consideration of this approach has centered on the validity of the "local cubic law" (equation (11)) governing fluid flow through rough fractures. *Brown et al.* [1995], *Mourzenko et al.* [1995], and *Oron and Berkowitz* [1998] found that use of the two-dimensional Reynolds equation gives significantly higher flow rates than are obtained by solving the three-dimensional Navier-Stokes equations. *Nicholl et al.* [1999] confirmed this general computational result by comparing the measured flow rates of analog fractures with flow rates calculated by the Reynolds equation. However, no consensus has emerged on the limits of applicability of the local cubic law (this issue is reviewed by *Zimmerman and Bodvarsson* [1996]). Of course, a fundamental restriction is that the streamlines be smooth with no eddies (so low Reynolds number), which requires the fracture surface profiles to be strongly correlated (for example, a self-affine fracture surface should have roughness exponent ζ closer to 1 than to 0). The present work is intended to obtain an algebraic relation between the hydraulic and electric apertures of rough fractures, where the latter are determined by a local flux equation analogous to equation (11) but with $d(\mathbf{r})^3$ replaced by $d(\mathbf{r})$. *Volik et al.* [1997] found this electric analogue to produce a larger effective conductivity than the three-dimensional Laplace equation. Thus, despite possibly poor values for d_h and d_e obtained from the two-dimensional Reynolds equation approach, it is reasonable to expect that a relation found between the two does indeed describe the transport properties of planar fractures.

[17] The Reynolds equation (12) is treated here by the walker diffusion method (WDM) [*Van Siclen*, 1999a] rather than solved by the finite difference method (FDM). The latter technique requires that a macroscopic fluid pressure difference be applied across the system in order to calculate transport properties; thus the FDM actually gives components of a permeability tensor, for example. However, while the flow properties of a rough fracture are indeed anisotropic (and become increasingly so as the fracture closes), there is no expected correlation between this anisotropy and the direction of the applied fluid pressure gradient; thus effective rather than tensor properties are desired for the present application. The WDM does not assume a macroscopic flow direction and so naturally gives effective transport properties. (It is evident from the WDM formalism that the effective permeability of a periodic planar fracture is the arithmetic average of the two permeability values for macroscopic transport in the two orthogonal directions of periodicity.) Other practical differences between the methods are that the FDM requires a discretization of the Reynolds equation that is effectively offset from that of the aperture field [e.g., *Romeu and Noetinger*, 1995; *Nicholl et al.*, 1999], while the WDM works directly with the given field; and the FDM is computer memory intensive while the WDM is CPU intensive.

[18] The walker diffusion method exploits the isomorphism between the Reynolds equation (12), with "local transport coefficients" $d(\mathbf{r})^3$, and the diffusion equation for a collection of noninteracting random walkers in the presence of a driving force. The walker density at each point $\mathbf{r}$ on a two-dimensional surface (corresponding to the plane of the fracture) is thus given by the value $d(\mathbf{r})^3$. The equilibrium population densities are maintained by the principle of detailed balance, which provides the following rule for walker diffusion over a digitized (square grid) surface: a walker at site (or pixel) i attempts a move to a randomly chosen adjacent site j during the time interval $\tau = 1/8$; this move is successful with probability $p_{ij} = d_j^3/(d_i^3 + d_j^3)$, where d_i and d_j are the fracture apertures at sites i and j, respectively. The path of a walker thus reflects the spatial variation of the fracture aperture and may be described by a diffusion coefficient $D_h \leq 1$ that is related to a "macroscopic transport coefficient" κ by

$$\kappa = \left\langle d(\mathbf{r})^3 \right\rangle D_h. \tag{14}$$

The diffusion coefficient is calculated from the standard relation $D_h = \langle R^2 \rangle/(4t)$, where the set $\{R\}$ of walker displacements, each occurring over the time interval t, comprises a Gaussian distribution that must necessarily be centered well beyond the permeability correlation length for the fracture [*Van Siclen*, 1999b].

[19] The significance of the quantity κ is that it satisfies the macroscopic relation

$$\langle \mathbf{q}(\mathbf{r}) \rangle = -\delta \frac{\kappa}{12\mu} \langle \nabla p(\mathbf{r}) \rangle, \tag{15}$$

which may be written in the more suggestive form

$$\mathbf{Q} = -\frac{\kappa}{12\mu\langle d(\mathbf{r})\rangle}\nabla P, \tag{16}$$

where $\mathbf{Q} = \langle \mathbf{q}(\mathbf{r})\rangle/(\delta\langle d(\mathbf{r})\rangle)$ is the volumetric flow rate of the fracture (this relation is derived in Appendix A). As equation (16) resembles Darcy's law (equation (13)), the quantity $\kappa/(12\langle d(\mathbf{r})\rangle)$ is identified with the permeability k_1. Thus

$$k_1 = \frac{\left\langle d(\mathbf{r})^3\right\rangle}{12\langle d(\mathbf{r})\rangle}D_h, \tag{17}$$

and the hydraulic aperture d_h is given by

$$d_h^3 = \left\langle d(\mathbf{r})^3\right\rangle D_h. \tag{18}$$

Equation (18) shows that the quantity d_h^3 is simply the effective value of the field composed of the local values $d(\mathbf{r})^3$. Combining equations (9) and (18) then gives $k \propto \langle d^3\rangle\, D_h$, where D_h accounts for the local fracture geometry (e.g., the spatial correlation of the fracture surface heights). The problem of determining the flow properties of a planar fracture is thus reduced to that of calculating the diffusion coefficient D_h of a random walker.

[20] The electrical properties of a fluid-filled planar fracture are found in similar manner. The local transport equation corresponding to the cubic law (equation (11)) is

$$\mathbf{i}(\mathbf{r}) = -\delta d(\mathbf{r})\sigma_0\nabla v(\mathbf{r}), \tag{19}$$

where $\mathbf{i}(\mathbf{r})$ and $v(\mathbf{r})$ are the local electrical current and potential, respectively. The conservation of flux then gives the two-dimensional Reynolds-type equation:

$$\nabla\cdot(d\nabla v) = 0. \tag{20}$$

The electrical analogue of equation (14) is

$$\Omega = \langle d(\mathbf{r})\rangle D_e, \tag{21}$$

where the walker diffusion coefficient $D_e \leq 1$ is determined in similar manner to D_h but with $p_{ij} = d_j/(d_i + d_j)$. The quantity Ω satisfies the macroscopic relation

$$\langle \mathbf{i}(\mathbf{r})\rangle = -\delta\Omega\sigma_0\langle\nabla v(\mathbf{r})\rangle, \tag{22}$$

which may be written in the form

$$\mathbf{J} = -\frac{\Omega\sigma_0}{\langle d(\mathbf{r})\rangle}\nabla V, \tag{23}$$

where $\mathbf{J} = \langle \mathbf{i}(\mathbf{r})\rangle/(\delta\langle d(\mathbf{r})\rangle)$ is the current density flux and ∇V is the applied potential gradient. This is just Ohm's law, so the quantity $\Omega\ \sigma_0/\langle d(\mathbf{r})\rangle$ is identified with the effective conductivity σ_1 of a planar fracture. Thus

$$\sigma_1 = \sigma_0 D_e \tag{24}$$

and the electric aperture of the fracture is

$$d_e = \langle d(\mathbf{r})\rangle D_e. \tag{25}$$

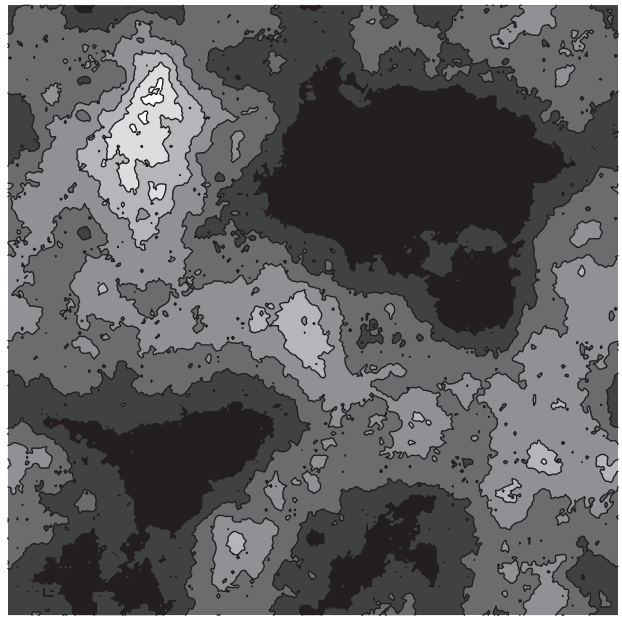

Figure 1. Example of a rough, planar fracture created from two self-affine surfaces having $\zeta = 0.8$. The view is normal to the fracture plane, with the black regions indicating where the two surfaces touch and the contours of increasingly lighter shading signifying increasingly greater aperture.

Equation (25) shows that d_e is simply the effective value of the aperture field. Combining equations (5) and (25) then gives $\sigma \propto \langle d\rangle\ D_e$. Equation (24) reflects the fact that both the electrical conductivity σ_1 and the walker diffusion coefficient obtained from the WDM are scale-invariant [*Van Siclen*, 1999b]. It may be noticed, particularly from the form of equation (24), that D_h and D_e are inversely related to the tortuosity of the fluid flow and electrical current streamlines, respectively, through a planar fracture; however, these tortuosities are subsumed in the effective apertures d_h and d_e and should not be confused with τ_h and τ_e above.

[21] Equations (17) and (24) for k_1 and σ_1, respectively, suggest no fundamental relationship between the permeability and the electrical conductivity of a planar fracture, despite the intentional similarity of their derivations. Thus it is necessary to calculate (or measure) the transport properties of a variety of planar fractures with different geometries to discover any phenomenological relationship.

[22] The planar fractures considered here are created from self-affine surfaces characterized by values for the roughness exponent ζ (this is just the Hurst exponent H, which is related to the fractal dimension D of the surface by $D = 3 - H$) and the variance $\sigma_h(L)^2$ of the distribution of surface heights, where L^2 is the planar area of a surface (note that the quantity $\sigma_h(L)/L^\zeta$, but not $\sigma_h(L)^2$, is surface size-independent). A typical ζ value for a real fracture surface is 0.8 [e.g., *Brown and Scholz*, 1985; *Schmittbuhl et al.*, 1995; *Bouchaud*, 1997].

[23] The computer-generated fracture surfaces are produced by the "successive random additions" method described by *Voss* [1985]. The two surfaces composing a fracture are periodic (with period L) and statistically identical and are uncorrelated with one another. Where they overlap (as the fracture closes), the mass is removed rather than redistributed. An example of a fracture with surfaces having $\zeta = 0.8$ is given in Figure 1. The view is normal to the fracture plane, with the black regions indicating where the two surfaces touch and the contours of increasingly lighter shading signifying increasingly greater aperture (the fractures used in the

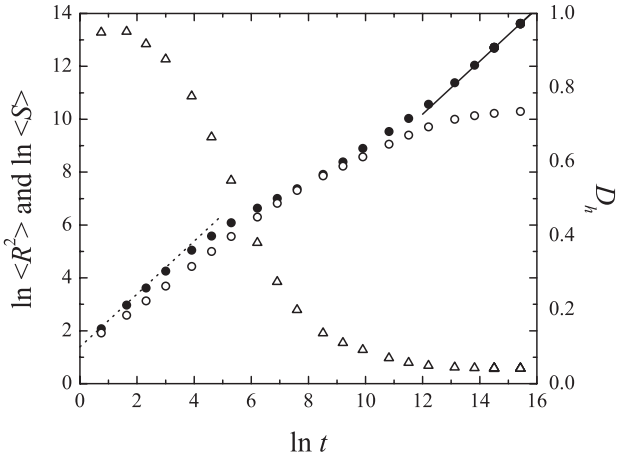

Figure 2. Typical data obtained by the walker diffusion method, in this case for a (periodic) planar fracture of size $L^2 = 256 \times 256$ and having surface roughness exponent $\zeta = 0.8$. The solid and open circles correspond to ln $\langle R^2 \rangle$ and ln $\langle S \rangle$ values, respectively, and the open triangles correspond to D_h values. Each data point is the average over 10^4 walks, each walk of duration t. To check the variability of the data, eight sets of 10^4 walks were taken for each of the two largest times t; in every case the eight data points overlap within the resolution of this plot. The coincidence of the solid circles with the solid line of slope 1 at the largest walk times t shows that the Gaussian regime has indeed been reached for the largest walker displacements R. The transition from the anomalous diffusion regime to the Gaussian regime occurs at the permeability correlation length ξ_h, which here is seen to approximately equal the periodicity L of the fracture. The coincidence of the solid circles with the dotted line of slope 1 (and y intercept ln 4) at the smallest walk times t indicates that the two fracture surfaces are locally parallel, reflecting the high degree of surface height correlation ($\zeta = 0.8$). The flattening of the curve of open circles at large walk times t indicates that essentially all the accessible sites ($S_A L^2$) were visited by the walker during the largest time interval t.

calculations were not contoured, of course). The connected regions of relatively large aperture constitute flow channels through the fracture. In this regard it is interesting to note that Figure 1 is unchanged when the fracture surface height variance $\sigma_h(L)^2$ is changed: the contour values are simply scaled by the ratio $\gamma = \sigma_h^{new}/\sigma_h^{old}$. Thus the walker diffusion coefficients D_h and D_e, being scale-invariant, are unchanged by the change in fracture surface height variance, while the aperture moments $\langle d^n \rangle$ are scaled by the factor γ^n. Evidently, D_h and D_e are functionals of the fracture surface roughness exponent ζ and the areal fraction $S_A < 1$ of the fracture plane that is accessible to the walkers (which is simply a measure of the degree of fracture closure) but not of the moments of the fracture surface height or aperture width distributions.

[24] For a given fracture a walker is placed at a random location on the fracture plane and allowed to diffuse according to the rules given above for a specified time t. This is repeated many times in order to obtain a large set $\{R\}$ of walker displacements from which the walker diffusion coefficient D_w (i.e., D_h or D_e) is calculated. (The variable residence time algorithm [*Van Siclen*, 1999a] was used to increase the computational efficiency of the walks.) The only complication to this simple scheme lies in ensuring that the set $\{R\}$ is taken in the Gaussian diffusion regime; that is, that the displacements R are much greater than the correlation length ξ for the system (ξ is specific to the transport property, so in general $\xi_h \neq \xi_e$). This was done by three ways, as illustrated in Figure 2. First, the Gaussian regime is identified as that region of the ln $\langle R^2 \rangle$ versus ln t plot where the data points fall on a straight line of slope 1. (Incidentally, that line has y intercept ln $(4D_w)$.) Second, for these periodic fractures with $\xi \leq L$, the number $S(t)$ of different sites visited by the walker over the time t must equal the number of accessible sites in the system (and so will have a constant value). Third, the Gaussian regime produces a constant value for D_w (those values for D_w calculated in the anomalous diffusion regime ($R < \xi$) are meaningless).

[25] Results of computations of d_e and d_h^3 for a variety of simulated, planar fractures are plotted in Figure 3. Each symbol identifies a set of fractures, where successive members of the set are obtained by further reducing the aperture of an initial fracture. Thus the data points of a set, going from right to left, correspond to a planar fracture under increasing pressure, and the slope of a curve drawn through those data points gives the value of the power law exponent r for that fracture. The straight lines with slopes 3, 2, and 1 are included in the log-log plot to show that $r \to 3$ for fractures with well separated surfaces (i.e., large aperture) and that $1 \leq r \leq 3$ in agreement with experimental observations. The slope r is clearly not constant for a set of fractures but decreases slowly with decreasing aperture (increasing pressure). However, r is effectively constant over the much narrower range of pressures that can be achieved experimentally (i.e., below the threshold pressure at which the rock responds inelastically). For reference, the first data point in each set corresponds to a fracture with S_A between 0.9 and 1, while the last data point corresponds to a fracture with S_A between 0.5 and 0.7 (for comparison, the two-dimensional site percolation threshold for a disordered conductor-insulator system occurs at $S_A = 0.59275$). The fact that all the data points lie on or above the superposed lines with slopes 3 and 2 indicates that $d_e \leq d_h \leq \langle d \rangle$ in general, in agreement with *Brown* [1989].

[26] These results are consistent with those obtained in the computational studies of planar fractures referenced above. *Brown* [1989, Figure 12] shows a plot similar to Figure 3 where the slope r is found to decrease from 3 to 2 as a planar fracture with $\zeta = 0.5$ is closed.

[27] The most striking feature of Figure 3 is the alignment of data points with slope 2. The significance of the slope (or power

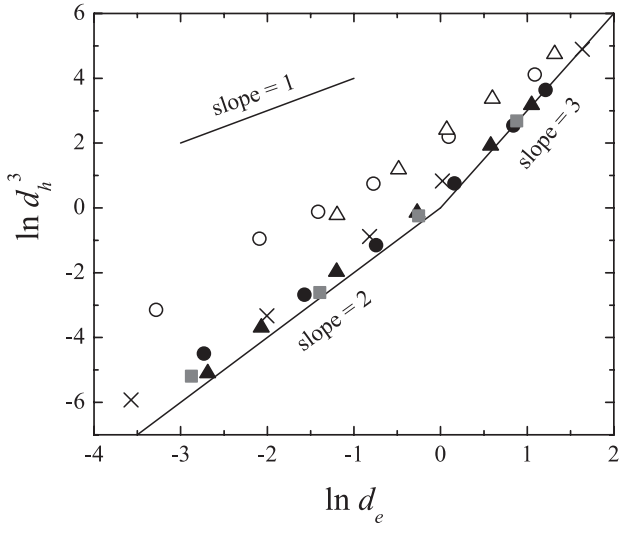

Figure 3. Computational results obtained for a variety of simulated, planar fractures with periodicity $L = 256$. The squares and triangles (circles) are data points for fractures with fracture surface roughness exponent $\zeta = 0.8$ (0). The solid (open) symbols indicate fractures created with a small (large) fracture surface height variance. The crosses are data points for fractures created from surfaces that are uncorrelated (i.e., surface heights are assigned randomly from a Gaussian distribution) and have a small height variance.

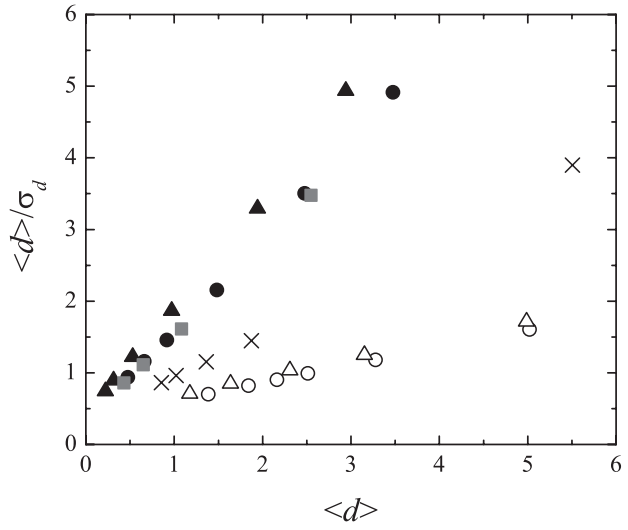

Figure 4. The ratio $\langle d\rangle/\sigma_d$, which is a crude indicator of the shape of the fracture void space, plotted against the average aperture $\langle d\rangle$. A small value of the ratio indicates that the void space is divided into distinct pores connected by narrow necks. Those points in Figure 3 that lie on a slope $r \leq 2$ have $\langle d\rangle/\sigma_d \leq 2$.

law exponent) 2 becomes apparent when the partially closed fracture is regarded as a three-dimensional porous material; that is, as a collection of connected pores all lying in the fracture plane (Figure 1 can certainly be viewed in this way). An equivalent channel network model for porous media (derived in Appendix B) yields the transport properties $\sigma \propto r_e^2$ and $k \propto r_h^2 \langle r^2\rangle$ for this configuration, where $\pi\langle r^2\rangle$ is the average cross-sectional area of the equivalent channel (or flow tube), and r_e and r_h are the electric and hydraulic radii, respectively. The proportionality constants, which contain the electric and hydraulic tortuosity factors, are little affected by a decrease in the fracture aperture. Use of the Reynolds approximation for linear flow tubes gives the additional relation $r_e = r_h$. Then for the extreme case where the connected pores form smooth, cylindrical tubes of uniform cross section, the equality $r_e^2 = r_h^2 = \langle r^2\rangle$ holds, and thus the permeability and electrical conductivity of the porous material follow the power law $k \propto \sigma^2$ as the pores are uniformly constricted. The opposite extreme is the case where the medium is composed of pores connected by very narrow necks. Then the effective cross sections πr_e^2 and πr_h^2 decrease much more rapidly than the average pore/neck cross section $\pi\langle r^2\rangle$, so that the latter is effectively constant and $k \sim \sigma^1$.

[28] Of course, it is the distribution of flow that determines the transport properties of a heterogeneous medium. Because flow paths without narrow necks will generally carry more flow than paths with narrow necks, the power law exponent is expected to be closer to 2 than to 1. Indeed, the relation $k \propto \sigma^2$ is found for artificial porous materials formed from fused glass beads, where each sample had a different porosity achieved by sintering [*Wong et al.*, 1984]; for alumina ceramic samples each with a different porosity [*Brouers and Ramsamugh*, 1986]; and for simulated, three-dimensional systems of packed, spherical grains at various consolidations, where the permeability was calculated by solving the linear Stokes equations and the conductivity was calculated by a method similar to the WDM [*Schwartz et al.*, 1993].

[29] This analysis suggests that when the partially closed fracture is regarded as a porous material, the value of the power law exponent r is constrained to lie between 2 and 1. Evidently, this structural transition is complete when the ratio $\langle d\rangle/\sigma_d$ has fallen to 2 (see Figure 4). The analysis also suggests that $r \rightarrow 1$ as the percolation threshold is approached; however, the pore network tortuosity factors, which have been assumed to be little affected by the changing fracture aperture, will certainly increase rapidly in this case. Thus this analysis cannot provide a prediction for r when the fracture is close to the percolation threshold. (It is perhaps useful to note here that the pore network tortuosity factors cannot be determined from the coefficients D_h and D_e obtained for a planar fracture.)

[30] The data points in Figure 3 are obtained by calculating the effective transport properties of the planar fractures. In practice, of course, the transport properties are measured after a fluid pressure or electrical potential difference is established across the system. Figure 5 presents results of computations of orthogonal components of d_e and d_h^3 for one of the sets of fractures considered in Figure 3. Clearly, the properties are increasingly anisotropic as the fracture closes and will produce a rather different value for r depending on the direction of the applied gradients in the plane of the fracture. Such anisotropy further complicates attempts to predict the geometry of a fracture given the transport properties, and vice versa. (Experiments by *Méheust and Schmittbuhl* [2000] clearly reveal the anisotropy of the flow properties of a nominally isotropic planar fracture.)

[31] It is important to note that Figure 3 is a parametric plot and so does not indicate a functional relationship between the hydraulic and electric transport properties. In particular, Figure 3 cannot be taken as evidence that the transport properties are influenced primarily by the variance σ_h^2 of the fracture surface height distribution (or the variance σ_d^2 of the aperture distribution) and very little by the spatial correlation of the surface heights (as specified here by the roughness exponent ζ). To see this, the dimensionless ratios $d_h/\langle d\rangle$ and $\langle d\rangle/\sigma_d$ calculated for the fractures presented in Figure 3 are plotted against one another in Figure 6. It is apparent that the open and solid triangles ($\zeta = 0.8$) define a single curve, as do the open and solid circles ($\zeta = 0$). This is because the fractures corresponding to the open and solid symbols are created from fracture surfaces that differ only in their height variance σ_h^2 (the former set of fractures has much larger σ_h^2 than the latter set); thus the dimensionless ratios scale by $\gamma/\gamma = 1$ in going from one such fracture to another, but this does not then imply that a simple relationship between $d_h/\langle d\rangle$ and $\langle d\rangle/\sigma_d$ can be found for fractures having a particular roughness exponent. For

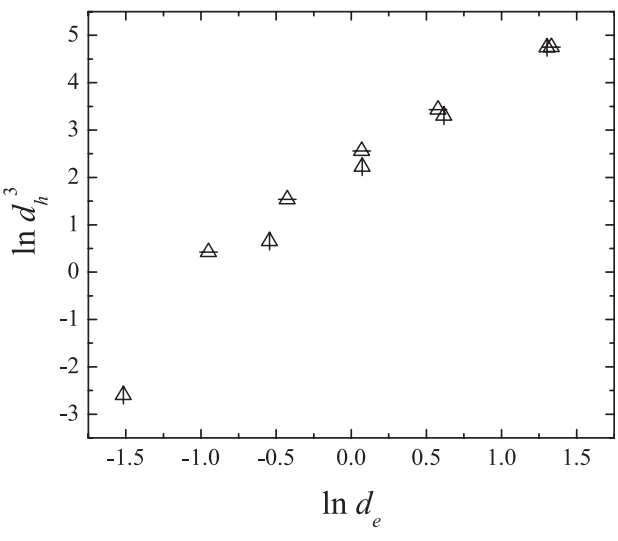

Figure 5. Illustration of the increasing anisotropy of the transport properties of a planar fracture as the fracture closes. This particular fracture, at $S_A = 0.8$, is shown in Figure 1. The orthogonal (in the plane of the fracture) components are distinguished by the horizontal and vertical lines superposed on the open triangles (this fracture produces the effective values indicated by the open triangles in Figure 3).

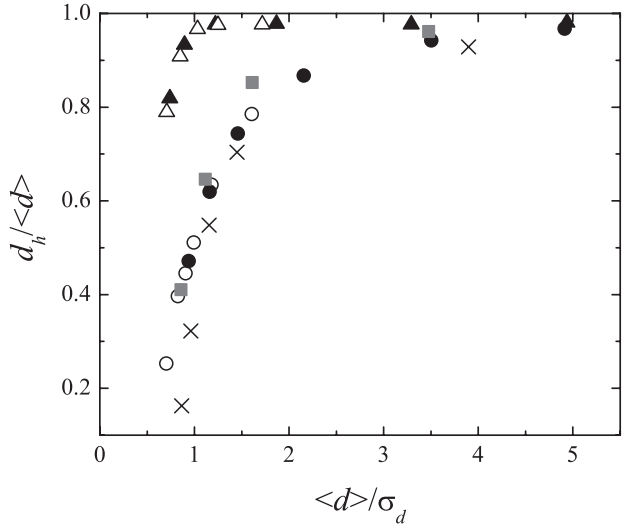

Figure 6. Dimensionless (i.e., normalized) hydraulic aperture plotted against the void shape factor $\langle d\rangle/\sigma_d$ for the fractures considered in Figure 3. No simple functional dependence is apparent.

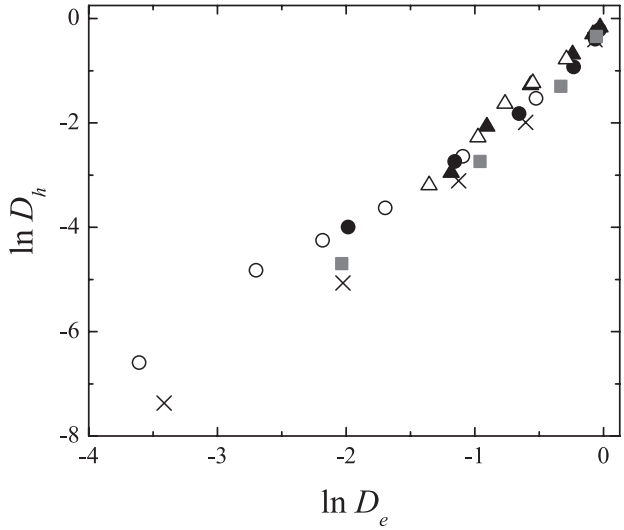

Figure 8. Calculated values of the walker diffusion coefficients D_h and D_e which reflect the spatial correlation of the fracture aperture (as derived from the spatial correlation of the fracture surface heights). These data suggest a general power law relation between the two coefficients.

example, the fractures corresponding to the solid squares have $\zeta = 0.8$ and surface height variance σ_h^2 only slightly larger than those fractures corresponding to the solid triangles yet produce a very different curve in Figure 6. Evidently, the transport properties of a planar fracture are not simple functions of the fracture surface height variance (or the fracture aperture variance). A different separation of geometrical properties results from the Reynolds equation approach: $k \propto d_h^3 = \langle d^3\rangle\ D_h$ and $\sigma \propto d_e = \langle d\rangle\ D_e$, where D_h and D_e are functionals of ζ and S_A. Figure 7 gives the calculated values of D_h for the sets of fractures considered in Figure 3 plotted against the S_A values for those fractures. These data are suggestive of the power law behavior $D_h \sim (S_A - S_A')^{\alpha} S_A^{-1}$, where S_A' is the percolation threshold for the fracture and the exponent α is a function of ζ. To verify or refute this conjecture would require calculations for a much larger number of fractures and is outside the scope of this paper. (However, it was checked that this power law relationship does indeed appear to hold for the set of fractures producing the crosses in Figure 3, where it is known that $S_A' = 0.59275$ for an infinite two-dimensional system.) The percolation properties of simulated fractures are discussed in detail by *Mourzenko et al.* [1996, 1999]. Note that the transport properties of two-dimensional linear fractures obtained by the Reynolds approximation are completely determined by the surface height or aperture distribution: $k \propto d_h^3 = \langle d^{-3}\rangle^{-1}$ and $\sigma \propto d_e = \langle d^{-1}\rangle^{-1}$.

[32] As mentioned above, the walker diffusion coefficients D_h and D_e are inversely related to the tortuosity of the fluid flow and electrical current streamlines, respectively, through the planar fracture. (In fact, if the walker were confined to a streamline, its diffusion coefficient would equal the inverse of the square of the streamline tortuosity.) Figure 8 shows that $D_h < D_e$ for every fracture and further that $D_h \propto D_e^{\beta}$ with $\beta \approx 2.3$ when all fractures are considered together.

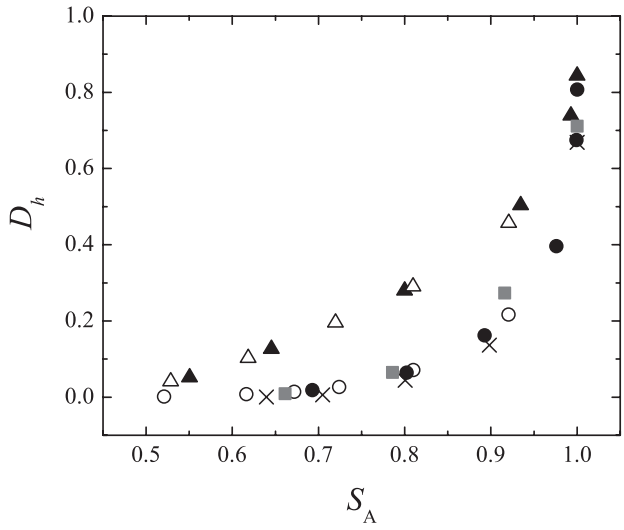

Figure 7. Walker diffusion coefficient D_h, which is a functional of the fraction S_A of the fracture plane accessible to the walker, plotted against S_A. These data suggest a power law relationship for S_A close to the percolation threshold.

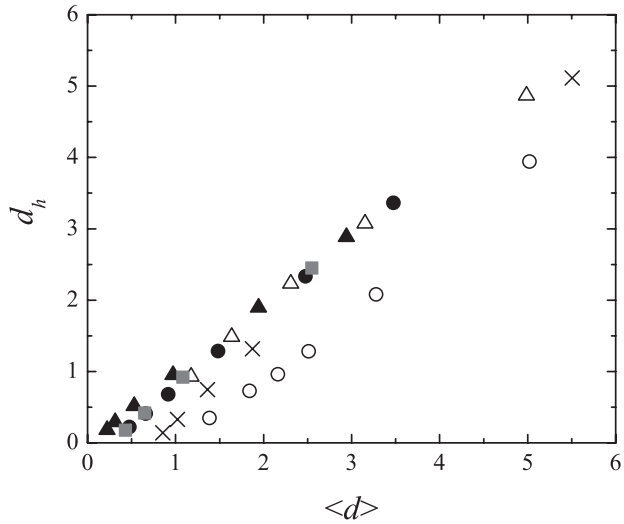

Figure 9. Hydraulic aperture d_h, which varies essentially linearly with the average aperture $\langle d\rangle$ and goes to zero for a nonzero value of $\langle d\rangle$. This offset causes the cubic law to fail at small $\langle d\rangle$.

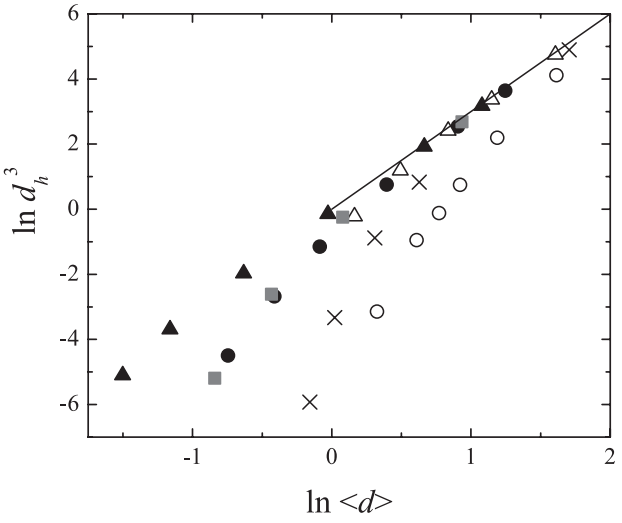

Figure 10. Demonstration that the hydraulic aperture d_h decreases as an increasingly higher power of the average aperture $\langle d \rangle$ as the planar fracture closes. Fractures that obey the cubic law produce points that lie on the straight line of slope 3.

[33] It is of interest to obtain a relation between the hydraulic aperture d_h and the average aperture $\langle d \rangle$ of a planar fracture. Figure 9 shows that in general, $d_h \propto (\langle d \rangle - \langle d \rangle_0)$, where the offset $\langle d \rangle_0$ is determined by the percolation threshold for the fracture. The offset is responsible for the breakdown of the cubic law for fluid flow as the fracture aperture decreases. This empirical "law" states that the flow rate per unit head difference varies as the third power of the fracture aperture. However, Darcy's law (equation (13)) gives

$$\mathbf{q}' = -w\langle d \rangle \frac{k_1}{\mu} \nabla P = -w \frac{d_h^3}{12\mu} \nabla P, \tag{26}$$

where $\mathbf{q}'$ is the volume of fluid discharged per unit time through the fracture (with cross-sectional area $w\ \langle d \rangle$). Then the cubic law is recovered when $d_h \propto \langle d \rangle$; that is, when $\langle d \rangle \gg \langle d \rangle_0$. When the average aperture $\langle d \rangle$ decreases toward the threshold value $\langle d \rangle_0$, the permeability must decrease as an increasingly higher power of $\langle d \rangle$ as shown in Figure 10. Indeed, *Nolte et al.* [1989] find powers of 7–10 for single, natural fractures close to their percolation threshold (as evidenced by the fractal character of the fluid flow paths). This trend will reverse in the inelastic regime if $\langle d \rangle_0$ moves to a smaller value (due to the creation of microcracks, for instance); such behavior has been observed by *Witherspoon et al.* [1980, Figure 8], *Durham and Bonner* [1994, Figure 5], and other researchers (*Renshaw* [1995, Figure 5] compiles data from a number of sources).

4. Discussion

[34] These calculations for simulated, planar fractures show that indeed the ratio d_h^3/d_e^r varies slowly with $\langle d \rangle$, as required by the equivalent channel network model to reproduce the general result $k(p) \propto \sigma(p)^r$ for fractured rock. The condition that τ_e^r/τ_h vary slowly with pressure is more difficult to address, if only because the fracture network tortuosity factors τ_h and τ_e are ill-defined. Of course, if the network structure is little affected by an applied pressure, the tortuosity factors are unchanged and the condition holds trivially. Indirect support for the general validity of the relation $\tau_h \propto \tau_e^r$ is provided by *Zhang and Knackstedt* [1995], who calculated the hydraulic and electric streamlines for a set of simulated, random porous materials. The hydraulic and electric tortuosity factors for the materials were obtained by weighing the measured tortuosity of each streamline by its volumetric flow to account for the distribution of flow among the streamlines. Their plot of the tortuosity factors as a function of the material porosity suggests a power law relation with exponent approximately equal to 2. Clearly, such a relation should be looked for in other systems to establish or refute its general validity.

[35] In any event, the network tortuosity factors introduced here have the great virtue that they permit the separation of the fracture network transport properties into local (d_h and d_e) and network (τ_h and τ_e) properties. In contrast, this distinction is not made in the equivalent channel model of *Walsh and Brace* [1984], which culminates in equation (1) above. The evidence presented here that the transport properties of planar fractures follow the power law $k(p) \propto \sigma(p)^r$ with $1 \leq r \leq 3$ cannot be reconciled with equation (1).

[36] An important implication of this work is that r values between 3 and 2 are simply "crossover" values that indicate a fracture undergoing the pressure-induced structural transition to a porous medium. By correlating the data in Figure 7 with that in Figure 3, it is apparent that the transition is complete when the fracture is 2 to 5 percent closed ($S_A = 0.98 - 0.95$). This result is consistent with observations by *Durham and Bonner* [1994] of departure from parallel-plate behavior at an S_A value between 0.996 and 0.91 in the case of an offset fracture in granite. In general, the transition will occur at a lower value of S_A the greater the fracture surface correlation (i.e., the larger the ζ value). Otherwise, the experimental value of the exponent r cannot be used to distinguish the fracture geometry.

[37] The treatment of planar fractures presented here has relied on the Reynolds equations. This enabled the application of the walker diffusion method (WDM), which produced analytic expressions for the transport properties. The n-dimensional Reynolds equation actually describes the flow of electrical current through an n-dimensional volume having spatially dependent conductivity. Thus Reynolds equations (12) and (20) for fluid and electrical current flow through a planar fracture produce streamlines that are precisely those for electrical current flowing across a two-dimensional conducting sheet with local conductivities $d(\mathbf{r})^3$ and $d(\mathbf{r})$, respectively. Viewed this way, fluid flow through a fracture, as described by equation (12), will certainly be more sensitive to local aperture variations (and so will take more tortuous paths) than the electrical current. Thus the Reynolds equations provide a crude, but qualitatively correct, model for fluid and electrical current flow. Of course, specific numerical results obtained from the Reynolds equation in each case will differ from those obtained by solving the Navier-Stokes equations and the Laplace equation, respectively.

[38] Finally, it is interesting to note that the effective conductivity of a lognormal distribution of conductivities in two dimensions equals the geometric mean of the distribution in the infinite volume limit [*Matheron*, 1967]. A fracture with lognormal aperture distribution (where the local values $d(\mathbf{r})$ are uncorrelated) will thus have an effective aperture d_e equal to the geometric mean of the aperture distribution, $\exp[\langle \ln d \rangle]$. The distribution of cubed values $d(\mathbf{r})^3$ is lognormal as well, so the effective value d_h^3 equals the geometric mean $\exp[\langle \ln d^3 \rangle]$. Then $d_e = d_h = \exp[\langle \ln d \rangle]$. The last equality was used by *Renshaw* [1995] to define the hydraulic aperture of a fracture; this definition proved successful in reproducing many numerical and experimental flow results.

Appendix A: Derivation of the Relation Between Local and Macroscopic Flow Rates

[39] Consider a planar fracture oriented such that the fracture plane is parallel to the x-y plane and the macroscopic fluid pressure gradient is in the y direction ($\mathbf{j}$). Then the volume of fluid discharged per unit time through the fracture is

$$q' = \int_0^w \frac{\mathbf{j}\bullet\mathbf{q}(x,y)}{\delta} dx \tag{A1}$$

and the cross-sectional area of the fracture normal to the macroscopic flow direction is

$$A = \int_0^w d(x,y)dx. \tag{A2}$$

The volumetric flow rate Q of the fracture is then

$$Q = \frac{q'}{A} = \frac{\langle \mathbf{j}\bullet\mathbf{q}(x,y)\rangle_x}{\delta\langle d(x,y)\rangle_x}, \tag{A3}$$

where the subscript x signifies that the averages are taken over the x coordinate. Since all cross sections normal to the fracture plane are statistically identical, and the components of $\mathbf{q}(\mathbf{r})$ normal to the macroscopic flow direction sum to zero, equation (A3) is equivalent to

$$\mathbf{Q} = \frac{\langle \mathbf{q}(\mathbf{r})\rangle}{\delta\langle d(\mathbf{r})\rangle}. \tag{A4}$$

Appendix B: Derivation of the Equivalent Channel Network Model for Porous Media

[40] In this model a porous material is comprised of connected, locally linear flow channels embedded in an impermeable (and insulating) matrix. The transport properties of such a network may be described in terms of the effective electric and hydraulic radii r_e and r_h, respectively, of the linear flow channels and the tortuosity factors τ_e and τ_h determined by the network structure.

[41] The electrical conductance g_1 of a single, fluid-filled, linear flow tube of length L is given by

$$g_1 = \sigma_0 \frac{\pi r_e^2}{L}, \tag{B1}$$

where r_e is the radius of a smooth, cylindrical tube that produces the same current as the linear flow tube for a given potential difference applied across the length of the tube. Then the electrical conductivity σ_1 of the single, linear flow tube is

$$\sigma_1 = \frac{g_1 L}{\pi\langle r^2\rangle} = \sigma_0 \frac{r_e^2}{\langle r^2\rangle}, \tag{B2}$$

where $\pi\langle r^2\rangle$ is the average cross-sectional area of the tube. The pore network formed by a parallel configuration of such flow tubes oriented in the direction of the applied field has conductivity $\sigma = \phi_0 \sigma_1$, where ϕ_0 is the volume fraction of the tubes. A more realistic network is created by removing this restriction on the tube orientation and allowing the tubes to bend, which reduces the electrical conductivity to

$$\sigma = \frac{(\phi_0\tau)\sigma_1}{\tau^2} = \frac{\sigma_0\phi_0}{\tau}\frac{r_e^2}{\langle r^2\rangle}, \tag{B3}$$

where the factor τ accounts for the increased tube lengths. It is convenient for the purpose of this derivation to apply the relation $N_A = \phi_0/(\pi\langle r^2\rangle)$, where N_A is the areal number density of pores intersecting a cross section of the material perpendicular to the applied potential gradient, to equation (B3). Then the electrical conductivity σ of the pore network is

$$\sigma = N_A \sigma_0 \frac{\pi r_e^2}{\tau_e}. \tag{B4}$$

This is an equivalent channel model in that the electric cross section πr_e^2 and the average cross section $\pi\langle r^2\rangle$ characterize the locally linear flow tubes that comprise the pore network, while τ_e may be regarded as a current path tortuosity factor determined by the structure of the network.

[42] An analogous expression may be derived for the permeability k of the pore network. In this case, the hydraulic conductivity k_1 of a single, linear flow tube is given by

$$k_1 = r_h^2/8, \tag{B5}$$

where r_h is the radius of a smooth, cylindrical tube that produces the same volumetric flow rate as the linear flow tube for a given fluid pressure difference applied across the length of the tube. Then the analogue of equation (B3) is the relation

$$k = \frac{\phi_0}{\tau}\frac{r_h^2}{8}, \tag{B6}$$

and the analogue of equation (B4) is the relation

$$k = N_A \frac{\pi r_h^2\langle r^2\rangle}{8\tau_h}. \tag{B7}$$

Expressions for σ_1 and k_1 may also be found by application of the Reynolds approximation. Equating these with equations (B2) and (B5), respectively, produces a useful relation between the effective radii r_e and r_h. The Reynolds approximation considers the linear flow tube to be comprised of n short segments, where the ith segment is a disc of radius r_i and length L/n. The electrical conductance g_i of that segment is

$$g_i = \sigma_0 \frac{\pi r_i^2}{(L/n)} \tag{B8}$$

(note that the conductivity $\sigma_i = \sigma_0$ as expected). Then the conductance g_1 of the flow tube is given by the relation

$$g_1^{-1} = \sum_{i=1}^{n} g_i^{-1}, \tag{B9}$$

and the electrical conductivity is

$$\sigma_1 = \frac{g_1 L}{\pi\langle r^2\rangle} = \sigma_0 \frac{n}{\langle r^2\rangle}\left[\sum_{i=1}^{n} r_i^{-2}\right]^{-1}, \tag{B10}$$

where $\pi\langle r^2\rangle$ is the average cross-sectional area of the tube. Similarly, the permeability k_i of the ith segment is

$$k_i = r_i^2/8 \tag{B11}$$

so that the permeability k_1 of the flow tube is

$$k_1 = n\left[\sum_{i=1}^{n} k_i^{-1}\right]^{-1} = \frac{n}{8}\left[\sum_{i=1}^{n} r_i^{-2}\right]^{-1}. \tag{B12}$$

Equating expressions (B2) and (B10) for σ_1, and expressions (B5) and (B12) for k_1, gives the relations

$$r_e^2 = r_h^2 = n\left[\sum_{i=1}^{n} r_i^{-2}\right]^{-1} = \left\langle r^{-2}\right\rangle^{-1} \tag{B13}$$

when the Reynolds approximation is used. Note that the effective radii r_e and r_h are primarily affected by the smallest members of the set $\{r_i\}$, that is, by the necks connecting the pores.

[43] It should be recognized that the equality of r_e and r_h (equation (B13)) is a consequence of defining r_h according to equation (B5). The more conventional definition of r_h is that it is the radius of a smooth, cylindrical tube that produces the same volume flow rate as the linear flow tube for a given fluid pressure difference applied across the length of the tube. Then equations (B6) and (B7) become

$$k = \frac{\phi_0}{\tau}\frac{r_h^4}{8\langle r^2\rangle} = N_A\frac{\pi r_h^4}{8\tau_h}. \tag{B14}$$

In this case the hydraulic radius is given by the relation

$$r_h^4 = \left\langle r^{-4}\right\rangle^{-1} \tag{B15}$$

when the Reynolds approximation is used.

[44] **Acknowledgments.** This work was supported in part by the U.S. Department of Energy, Office of Environmental Management, under U.S. DOE Idaho Operations Office contract DE-AC07-99ID13727.

References

Bernabe, Y., Comparison of the effective pressure law for permeability and resistivity formation factor in Chelmsford granite, *Pure Appl. Geophys.*, *127*, 607–625, 1988.

Bouchaud, E., Scaling properties of cracks, *J. Phys. Condens. Matter*, *9*, 4319–4344, 1997.

Brouers, F., and A. Ramsamugh, Relation between conductivity and fluid flow permeability in porous alumina ceramics, *Solid State Commun.*, *60*, 951–953, 1986.

Brown, S. R., Fluid flow through rock joints: The effect of surface roughness, *J. Geophys. Res.*, *92*, 1337–1347, 1987.

Brown, S. R., Transport of fluid and electric current through a single fracture, *J. Geophys. Res.*, *94*, 9429–9438, 1989.

Brown, S. R., and C. H. Scholz, Broad bandwidth study of the topography of natural rock surfaces, *J. Geophys. Res.*, *90*, 12,575–12,582, 1985.

Brown, S. R., H. W. Stockman, and S. J. Reeves, Applicability of the Reynolds equation for modeling fluid flow between rough surfaces, *Geophys. Res. Lett.*, *22*, 2537–2540, 1995.

David, C., Geometry of flow paths for fluid transport in rocks, *J. Geophys. Res.*, *98*, 12,267–12,278, 1993.

Durham, W. B., and B. P. Bonner, Self-propping and fluid flow in slightly offset joints at high effective pressures, *J. Geophys. Res.*, *99*, 9391–9399, 1994.

Katsube, T. J., and J. B. Walsh, Effective aperture for fluid flow in microcracks, *Int. J. Rock Mech. Min. Sci. Geomech. Abstr.*, *24*, 175–183, 1987.

Matheron, G., *Elements Pour une Theorie des Milieux Poreux*, *Rev. Inst. Fr. Pét.*, *22*, 443 pp., Masson, Paris, 1967.

Méheust, Y., and J. Schmittbuhl, Flow enhancement of a rough fracture, *Geophys. Res. Lett.*, *27*, 2989–2992, 2000.

Moreno, L., Y. W. Tsang, C. F. Tsang, F. V. Hale, and I. Neretnieks, Flow and tracer transport in a single fracture: A stochastic model and its relation to some field observations, *Water Resour. Res.*, *24*, 2033–2048, 1988.

Mourzenko, V. V., J.-F. Thovert, and P. M. Adler, Permeability of a single fracture; validity of the Reynolds equation, *J. Phys. II*, *5*, 465–482, 1995.

Mourzenko, V. V., J.-F. Thovert, and P. M. Adler, Geometry of simulated fractures, *Phys. Rev. E*, *53*, 5606–5626, 1996.

Mourzenko, V. V., J.-F. Thovert, and P. M. Adler, Percolation and conductivity of self-affine fractures, *Phys. Rev. E*, *59*, 4265–4284, 1999.

Nicholl, M. J., H. Rajaram, R. J. Glass, and R. Detwiler, Saturated flow in a single fracture: Evaluation of the Reynolds equation in measured aperture fields, *Water Resour. Res.*, *35*, 3361–3373, 1999.

Nolte, D. D., L. J. Pyrak-Nolte, and N. G. W. Cook, The fractal geometry of flow paths in natural fractures in rock and the approach to percolation, *Pure Appl. Geophys.*, *131*, 111–138, 1989.

Oron, A. P., and B. Berkowitz, Flow in rock fractures: The local cubic law assumption reexamined, *Water Resour. Res.*, *34*, 2811–2825, 1998.

Patir, N., and H. S. Cheng, An average flow model for determining effects of three-dimensional roughness on partial hydrodynamic lubrication, *J. Lubrication Technol.*, *100*, 12–17, 1978.

Renshaw, C. E., On the relationship between mechanical and hydraulic apertures in rough-walled fractures, *J. Geophys. Res.*, *100*, 24,629–24,636, 1995.

Romeu, R. K., and B. Noetinger, Calculation of internodal transmissivities in finite difference models of flow in heterogeneous porous media, *Water Resour. Res.*, *31*, 943–959, 1995.

Schmittbuhl, J., F. Schmitt, and C. Scholz, Scaling invariance of crack surfaces, *J. Geophys. Res.*, *100*, 5953–5973, 1995.

Schwartz, L. M., N. Martys, D. P. Bentz, E. J. Garboczi, and S. Torquato, Cross-property relations and permeability estimation in model porous media, *Phys. Rev. E*, *48*, 4584–4591, 1993.

Thompson, M. E., and S. R. Brown, The effect of anisotropic surface roughness on flow and transport in fractures, *J. Geophys. Res.*, *96*, 21,923–21,932, 1991.

Van Baak, D. A., Variational alternatives to Kirchhoff's loop theorem in dc circuits, *Am. J. Phys.*, *67*, 36–44, 1999.

Van Siclen, C. D., Walker diffusion method for calculation of transport properties of composite materials, *Phys. Rev. E.*, *59*, 2804–2807, 1999a.

Van Siclen, C. D., Anomalous walker diffusion through composite systems, *J. Phys. A*, *32*, 5763–5771, 1999b.

Volik, S., V. V. Mourzenko, J.-F. Thovert, and P. M. Adler, Thermal conductivity of a single fracture, *Transp. Porous Media*, *27*, 305–326, 1997.

Voss, R. F., Random fractal forgeries, in *Fundamental Algorithms for Computer Graphics, NATO ASI Ser.*, vol. F17, edited by R. A. Earnshaw, pp. 805–835, Springer-Verlag, New York, 1985.

Walsh, J. B., and W. F. Brace, The effect of pressure on porosity and the transport properties of rock, *J. Geophys. Res.*, *89*, 9425–9431, 1984.

Witherspoon, P. A., J. S. Y. Wang, K. Iwai, and J. E. Gale, Validity of cubic law for fluid flow in a deformable rock fracture, *Water Resour. Res.*, *16*, 1016–1024, 1980.

Wong, P.-Z., J. Koplik, and J. P. Tomanic, Conductivity and permeability of rocks, *Phys. Rev. B*, *30*, 6606–6614, 1984.

Zhang, X., and M. A. Knackstedt, Direct simulation of electrical and hydraulic tortuosity in porous solids, *Geophys. Res. Lett.*, *22*, 2333–2336, 1995.

Zhang, X., M. A. Knackstedt, and M. Sahimi, Fluid flow across mass fractals and self-affine surfaces, *Physica A*, *233*, 835–847, 1996.

Zimmerman, R. W., and G. S. Bodvarsson, Hydraulic conductivity of rock fractures, *Transp. Porous Media*, *23*, 1–30, 1996.

Zimmerman, R. W., S. Kumar, and G. S. Bodvarsson, Lubrication theory analysis of the permeability of rough-walled fractures, *Int. J. Rock Mech. Min. Sci. Geomech. Abstr.*, *28*, 325–331, 1991.

C. D. Van Siclen, Idaho National Engineering and Environmental Laboratory, P. O. Box 1625, Idaho Falls, ID 83415-2211, USA. (cvs@inel.gov)